Advanced Magnetic Resonance Imaging (MRI) of Brain

9

Navdeep Kaur ⓘ, Soumya Swaroop Sahoo,
and Shailendra Singh Rana

Abstract

Magnetic Resonance Imaging (MRI) uses the principle of nuclear magnetic resonance to generate high-resolution images of brain. Due to abundance of water in human body, current MR imaging is based on proton imaging. MRI enables non-invasive structural as well as functional evaluation of brain parenchyma. T_1WI provide detailed structural evaluation of brain. Advanced sequences such as Diffusion Weighted Imaging (DWI), MR Perfusion, MR Spectroscopy, Diffusion Tensor Imaging and functional MRI enable the evaluation of metabolic, haemodynamic and cytoarchitecture of brain parenchyma in a non-invasive manner. This book chapter aims to provide insight into basic and various advanced MRI sequences along with its potential applications in neuroimaging.

Keywords

Magnetic Resonance Imaging · MR perfusion · MR spectroscopy · DTI · Functional MRI

N. Kaur (✉)
Department of Radiodiagnosis, All India Institute of Medical Sciences, Bathinda, Punjab, India

S. S. Sahoo
Department of Community and Family Medicine, All India Institute of Medical Sciences, Bathinda, Punjab, India

S. S. Rana
Department of Dentistry, All India Institute of Medical Sciences, Bathinda, Punjab, India

9.1   Introduction

The fine spatial resolution and non-invasiveness of Magnetic Resonance Imaging (MRI) makes it an integral component of the algorithm for evaluating patients with any neurological disease. Nowadays, MRI is not just limited to provide the anatomical details of tissues. Many advanced MRI sequences are being introduced to provide information about the cytoarchitecture, metabolic, haemodynamic and functional status of tissues to investigate the disease at molecular level.

9.2   Basic Principle

MRI is used to generate high-resolution images of human body. MRI is established on the principle of nuclear magnetic resonance (NMR). The two fundamental principles of NMR are as follows:

- Atoms with odd number of protons or neutrons have a spin.
- A moving electric charge generates a magnetic field.

Human body has many atoms such as ^1H, ^{13}C, ^{19}F, ^{23}Na and ^{31}P that can be used for MR imaging.

Currently, MR is primarily based on proton imaging. Hydrogen atom has only single proton, so one H^+ ion = one proton. Hydrogen ions are present in abundance in human body as water. So, out of all nuclei H^+ ion gives most intense signal on MR imaging (Fig. 9.1).

To localize from where the signal is coming from human body, three additional magnetic fields are superimposed on the principal magnetic field in *X*, *Y* and *Z* axes. These are called gradient fields which vary in strength with varying location. Slice selection gradient is used to select the slice and is sent at the time of Radiation Frequency (RF) pulse. Phase encoding gradient is turned on briefly after slice selection gradient. Frequency encoding/read out gradient is sent at the time of signal reception.

TR (Time to Repeat)—Time period between two RF pulses.
TE (Time to Echo)—Time gap between the start of RF pulse and reception of signal.

Varying combinations of TR and TE are used to generate different MR images.

T_1-weighted images—Short TR and short TE.
T_2-weighted images—Long TR and long TE.
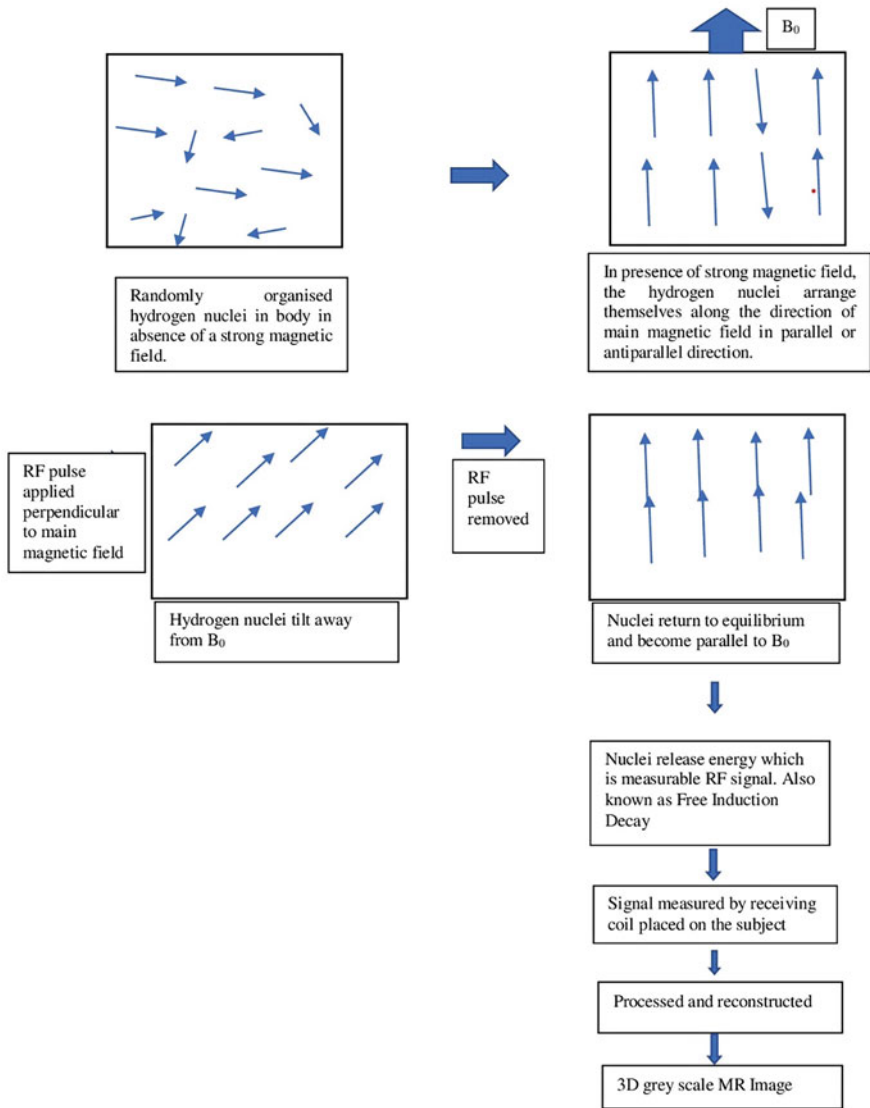Proton density images—Long TR and short TE.

Fig. 9.1 Generation of magnetic resonance signal

9.3   Various MR Sequences

9.3.1   T$_1$ Weighted Images (T$_1$WI)

Short Repetition Time (TR) and short Time to Echo (TE) generate T$_1$WI. Fluid appears dark and fat appears bright on T$_1$WI (Fig. 9.2a). T$_1$WI best depict the normal anatomy of brain parenchyma. Grey matter appears intermediate in signal intensity, while white matter appears hyperintense as compared to grey matter. Gadolinium decreases T$_1$ of the tissues and appear bright on T$_1$WI. So, post-contrast images can be used for depiction of vascular changes. In various pathologies such as tumours and inflammation, breakdown of blood–brain barrier can lead to leakage of contrast into the brain parenchyma causing its enhancement and thus localization of pathology on post-contrast T$_1$WI.

9.3.2   T$_2$ Weighted Images (T$_2$WI)

Long TR and long TE generate T$_2$WI. Fluid appears bright and fat appears dark on T$_2$WI. Grey matter appears intermediate signal intensity, while white matter appears hypointense as compared to grey matter (Fig. 9.2). As most pathologies are associated with cerebral oedema, i.e. increased signal on T$_2$WI, they are more easily picked up on T$_2$WI.

9.3.3   Fluid Attenuation Inversion Recovery (FLAIR) Sequence

FLAIR is a special inversion recovery sequence which supresses the cerebrospinal fluid (CSF) (Fig. 9.2). So, it enables us to detect cerebral oedema without glaring high signal from CSF particularly in periventricular regions and in periphery near
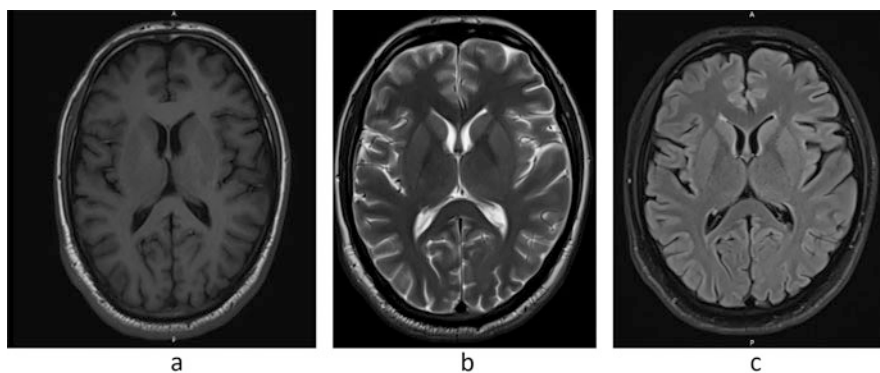

Fig. 9.2 Axial MRI of brain at level of lateral ventricles showing cerebrospinal fluid as dark signal on T$_1$WI (**a**), bright on T$_2$WI (**b**) and suppression on FLAIR (**c**) images

sulcal spaces. FLAIR sequence is very useful in evaluating various diseases of central nervous system such as infarction, demyelination and subarachnoid haemorrhage in trauma patients [1–3]. Post-contrast FLAIR images have been used for evaluating leptomeningeal diseases as early meningitis as it enables us to detect which even subtle meningeal enhancement [4].

9.3.4 Diffusion Weighted Imaging (DWI)

DWI is based on the principle of measuring Brownian, i.e. random motion of water molecules in each voxel of tissue. Since microarchitecture of cerebral tissues affect the Brownian motion of water molecules, it may be used to study the cellular integrity. Any pathology such as inflammation or mass lesion restricts the free motion of water molecules in tissues causing bright signal on DWI.

However, few tissues which are bright on T_2WI, appear bright on DWI without any apparent reduced water diffusion. This is specified as T_2 shine through. Misinterpretation of T_2 shine through for true restricted diffusion can be avoided by using Apparent Diffusion Coefficient (ADC) maps. These ADC images demonstrate actual diffusion values of tissues. Any pathology appears dark on ADC images.

DWI plays a major role in evaluating the following diseases [5–7]:

1. Diagnosis of early stroke, distinguishing acute from chronic stroke and stroke mimics—the vasogenic oedema in acute stroke restricts the free motion of water molecules in affected brain tissue, thus appearing bright on DWI images and dark on ADC maps (Fig. 9.3).
2. Differentiating epidermoid cyst from arachnoid cyst—both the lesions will appear hyperintense on T_2WI. Epidermoid cyst shows diffusion restriction on DWI/ADC as compared to arachnoid cyst which does not show diffusion restriction.
3. Assessment of active demyelinating lesions as in multiple sclerosis which will show restricted diffusion as compared to the chronic plaques.
4. Grading of diffuse gliomas and meningiomas—extent of tumour cellularity is used for quantitative assessment with DWI. Glioma grade is inversely related with ADC values [8]. Higher the tumour grade—more the cellularity, more the diffusion restriction and lower the ADC values.

9.3.5 Susceptibility Weighted Imaging (SWI)

Compounds having paramagnetic, diamagnetic and ferromagnetic properties distort the local magnetic field altering the phase of local tissues and thus resulting in change of signal [9]. SWI aids in detecting structures that have separate susceptibility in comparison to the surrounding structures like deoxygenated blood, ferritin, haemosiderin and calcium [10]. Calcium can be easily picked up on SWI images which may not be visible on routine images.
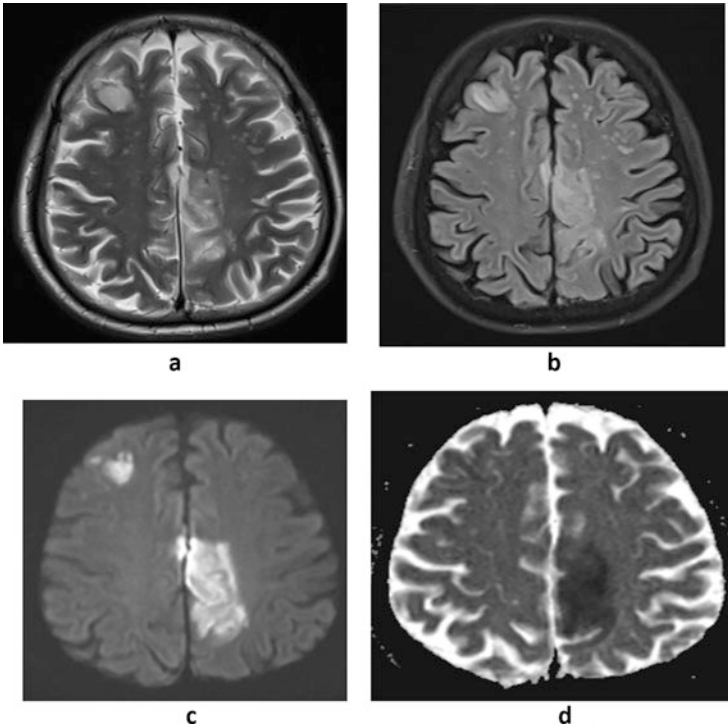
Fig. 9.3 Axial MRI of brain showing area of altered signal intensity involving right frontal lobe and left parietal lobe. It appears hyperintense on T_2WI (**a**) and FLAIR (**b**) images. The area shows restriction on DWI (**c**) and ADC (**d**) images consistent with acute infarct

SWI is also known as high-resolution blood oxygen level-dependent (BOLD) venography. Paramagnetic deoxyhaemoglobin in veins cause shift in resonant frequency between venous channels and the surrounding brain parenchyma thus aiding in detecting various vascular malformations such as deep venous anomaly.

It is exquisitely sensitive in detecting small haemorrhagic contusions in traumatic brain injury. Identification of small haemorrhages along with their location provides valuable information concerning the mechanism of injury and prognosis of the patient [11].

SWI has the ability to detect minute bleeds within the infarct thus precluding the use of revascularization therapies in case of early haemorrhagic transformation of infarct [12] (Fig. 9.4).

9.3.6   MR Perfusion Imaging

MR perfusion imaging enables us to non-invasively measure cerebral perfusion through assessment of multiple haemodynamic parameters such as cerebral blood
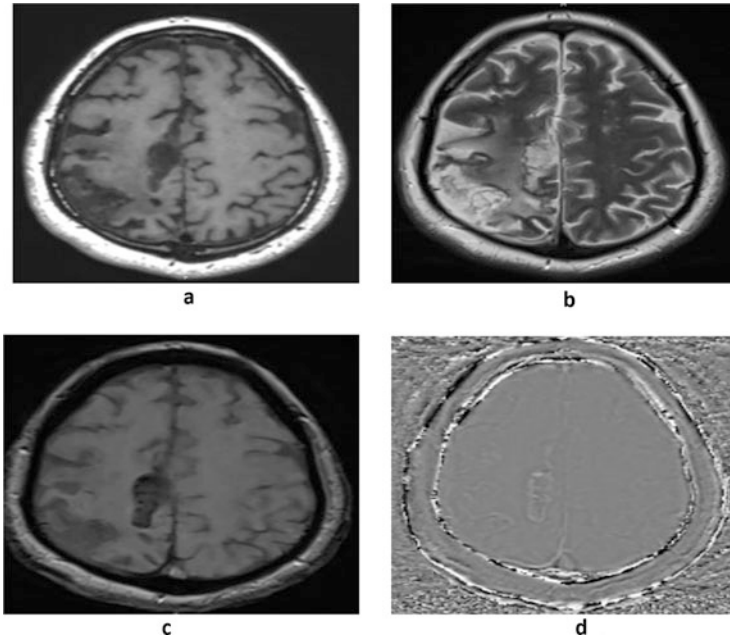
Fig. 9.4 Axial MRI of brain showing area of altered signal intensity involving right parietal lobe. It is hypointense on T_1WI (**a**), and hyperintense on T_2WI (**b**) consistent with infarct. Foci of blooming seen in it in right parasagittal location on SWI (**c**) and appearing bright on phase images (**d**) indicating haemorrhagic transformation

volume, cerebral blood flow and mean transit time. Exogenous tracer method involving the use of paramagnetic contrast material may be used or magnetically labelled blood may be used as endogenous tracer material [13].

9.3.6.1 Dynamic Susceptibility Contrast (DSC) MR Perfusion

It is the most frequently used technique for MR perfusion study. It uses the regional susceptibility-induced signal loss due to paramagnetic contrast material (such as gadolinium) on T_2 or T_2* WI. Gadolinium containing contrast medium is injected intravenously and rapid repeat sequences of brain are acquired during the first pass of the contrast. Signal in each voxel represents the intrinsic tissue T_2/T_2* signal attenuated by susceptibility induced signal loss proportional to the amount of contrast in the vessels [14, 15].

After image acquisition, signal intensity-time curve is generated from area of interest and various parameters such regional cerebral blood volume, cerebral blood flow and mean transit time can be calculated. Also, we can use these values to generate coloured maps of area of interest.

9.3.6.2 Dynamic Contrast Enhanced (DCE) MR Perfusion

DCE MR perfusion calculates cerebral perfusion parameters by assessing T_1 shortening effects of gadolinium. Gadolinium-based contrast media is injected intravenously and repeated T_1WI are obtained. The most frequently calculated parameter is k-trans, i.e. measure of capillary permeability.

9.3.6.3 Arterial Spin Labelling (ASL)

It does not require use of any exogenous contrast medium. Water molecules in incoming blood are magnetically tagged using a radiofrequency pulse which saturates the water protons. Labelled or tagged images and control images are obtained in which the signal from static tissues is identical but of inflowing blood is different. Subtraction of labelled and control images removes the signal from static tissues and the remaining signal measures perfusion which is proportional to cerebral blood flow (CBF).

Compared to other methods, ASL has very low signal-to-noise ratio but is very useful in paediatric patients or patients with impaired renal function who require serial follow-ups [16].

9.3.6.4 Uses

- In acute stroke, perfusion-diffusion mismatch can help in identifying ischaemic penumbra, i.e. surrounding viable ischaemic tissue which is at risk of infarction [17, 18]. Area with reduced cerebral blood volume and cerebral blood flow and increased mean transit time represents the infarcted core as well as the reversible surrounding ischaemic tissue, whereas the area with diffusion restriction represents irreversibly infarcted core.
- Cerebral blood volume maps help us to assess neovascularity within the tumour that correlates well with tumour grade and malignant histology and to localize tumour area expected to yield positive results on stereotactic biopsy. It can enable us to differentiate radiation necrosis from recurrent tumour.
- While evaluating patients with migraine headaches, during the aura, patients show decreased cerebral blood flow and blood volume as compared to post-aural state.
- Its role is being evaluated in dementia patients. Alzheimer's disease patients have shown decreased cerebral blood volume in the temporal and parietal lobes. The results are consistent with findings of single-photon emission computerized tomography (SPECT) studies in these patients [19, 20].

9.3.7 Magnetic Resonance Spectroscopy (MRS)

^{1}H-MRS is an advanced non-invasive imaging tool which provides information about biochemical composition of tissue being imaged. The main metabolites of brain parenchyma include *N*-acetyl aspartate (NAA), Choline (Cho) and Creatine (Cr) which show peaks at different parts per million (ppm) (Fig. 9.5). The metabolic changes precede the anatomical changes during the development of disease as well
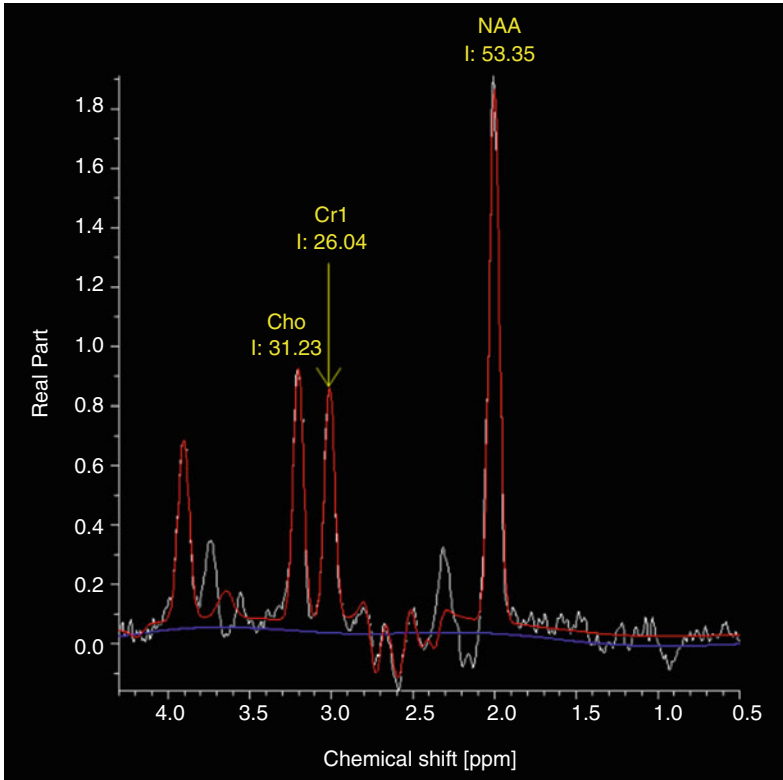
Fig. 9.5 MR spectroscopy image of normal brain parenchyma showing *N*-acetyl aspartate (NAA) peak at 2.01 ppm, Choline peak at 3.20 ppm and Creatine peak at 3.03 ppm

as during response to treatment. So, MRS is a highly sensitive tool to assess these changes at an early stage (Table 9.1).

9.3.8 Diffusion Tensor Imaging (DTI)

DTI is utilized to map and characterize three-dimensional diffusion of water molecules as a function of spatial localization [37, 38]. Diffusion of water in biological tissues is produced by random thermal fluctuations and is hindered by cellular structures and cell membranes. Thus, it leads to anisotropy, i.e. varying magnitude in different directions.

In cerebral white matter, diffusion of water is relatively less restricted in the direction parallel to fibre orientation, while it is exceedingly impeded in the direction perpendicular to the white matter. Major diffusion eigenvector is presumed to be parallel to the orientation of white matter tracts in homogenous white matter

Table 9.1 Magnetic resonance spectroscopy peaks

Metabolite	Peaks at	Significance
NAA (*N*-acetyl aspartate)	2.01 ppm[a]	Recognized as neuronal marker as it is predominantly found in neurons, axons and dendrites in the central nervous system [21]. Elevated in Canavan's Disease [22].
Choline	3.20 ppm	Elevated in gliomas and in active demyelination [23]. Low levels in hepatic encephalopathy [24].
Lactate	1.31 ppm	Not detectable under normal conditions in brain parenchyma. Elevated in acute hypoxia, ischaemic injury, in brain tumours or mitochondrial diseases [25–30].
Myo-inositol	3.5–3.6 ppm	Reduced in hepatic encephalopathy [31]. Elevated in Alzheimer's dementia and demyelinating diseases [32, 33].
Creatine	3.03 ppm	Involved in energy metabolism. Glial cells have higher concentration than neurons [34]. Higher levels of creatine in cerebellum as compared to supratentorial brain parenchyma.
Glutamate and glutamine	2.2–2.4 ppm	Most abundant amino acid in brain. Glutamate is the dominant neurotransmitter. Glutamate is elevated in multiple sclerosis plaques [35]. Elevated glutamine is found in hepatic encephalopathy and Reye's syndrome [31, 36].

[a]ppm: parts per million

[39]. Tractography algorithms are used to generate estimates of the white matter trajectories in human brain.

Tractography methods are applied primarily to generate reconstructions of the major projection pathways, i.e. corticospinal tract, corona radiata, commissural pathways (corpus callosum and anterior commissure) and also association pathways such as arcuate fasciculus, uncinate fasciculus and inferior longitudinal fasciculus [40–44] (Fig. 9.6). Any pathology causing change in tissue microarchitecture alters the anisotropy, thus making DTI a highly efficient tool for indicating the effects of disease on tissue microarchitecture (Fig. 9.7). DTI has a high sensitivity but low specificity which poses a unique challenge to its applications in neurology.

9.3.8.1 Uses

1. Brain tumours—The customary clinical application of DTI is characterization of white matter tracts in persons with brain tumours. DTI maps and tractography help to localize white matter fibre tracts involved in critical functions such as vision, language and motion [44–46]. This information enables the neurosurgeon to plan the surgery accordingly minimizing damage to these critical tracts such as corticospinal tracts [47].
2. Stroke—Diagnosis and characterization of acute ischaemic lesions can be done in the brain parenchyma. During acute phase of the disease, the mean diffusivity significantly reduces in the lesion [48]. After few days (5–7 days), the mean diffusivity normalizes and significantly increases in chronic phase when

Fig. 9.6 Diffusion tractography image showing anteroposterior fibres as green, transverse fibres as red and craniocaudal fibres as blue in color
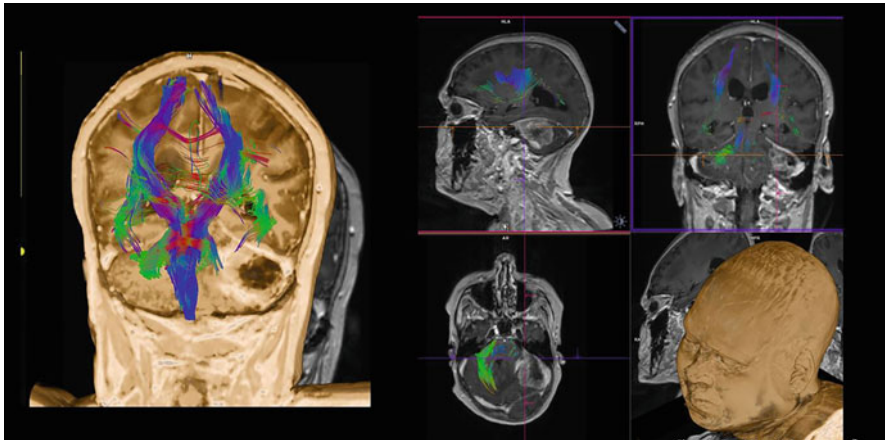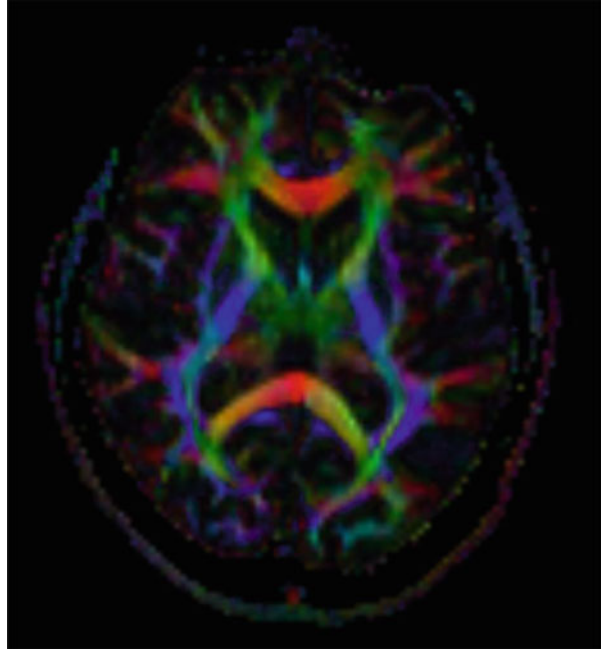

Fig. 9.7 Diffusion tractography image of brain showing destruction of left middle cerebellar peduncle by the mass lesion in left cerebellar hemisphere

encephalomalacia ensues. Fractional anisotropy increases during the acute phase and decrease below the baseline level during chronic phase [49–51].

3. Demyelination—Parallel organization of white matter fibres forms the ground for diffusion anisotropy and myelin modulates the degree of anisotropy [52]. Any

disease process causing dysmyelination or demyelination will cause increased radial diffusivity and decrease in anisotropy. This has been particularly seen in relapsing-remitting multiple sclerosis, periventricular frontal white matter in early Alzheimer's disease, in periventricular white matter in hydrocephalus, in extratemporal white matter in temporal lobe epilepsy, in genu of corpus callosum in cocaine addicts and in the corpus callosum of patients with autism [53–58].

9.3.9 Functional MRI (fMRI)

fMRI as a technique is used to obtain functional imaging by visualizing alterations in blood flow in cerebral cortex in response to stimuli or actions (Fig. 9.8).

In this technique, the patient is instructed to perform a particular task. In response to the task, there is an increase in regional cortical activity which increases the oxygen requirement of the activated cortex leading to drop in oxyhaemoglobin concentration and an increase in deoxyhaemoglobin concentration. Following a delay of 2–6 s, there is an increase in cerebral blood flow (CBF) thus washing away deoxyhaemoglobin. This rebound in tissue oxygenation is measured [59, 60].

fMRI utilizes the difference in paramagnetic properties of oxyhaemoglobin and deoxyhaemoglobin. Deoxygenated haemoglobin is basically paramagnetic causing
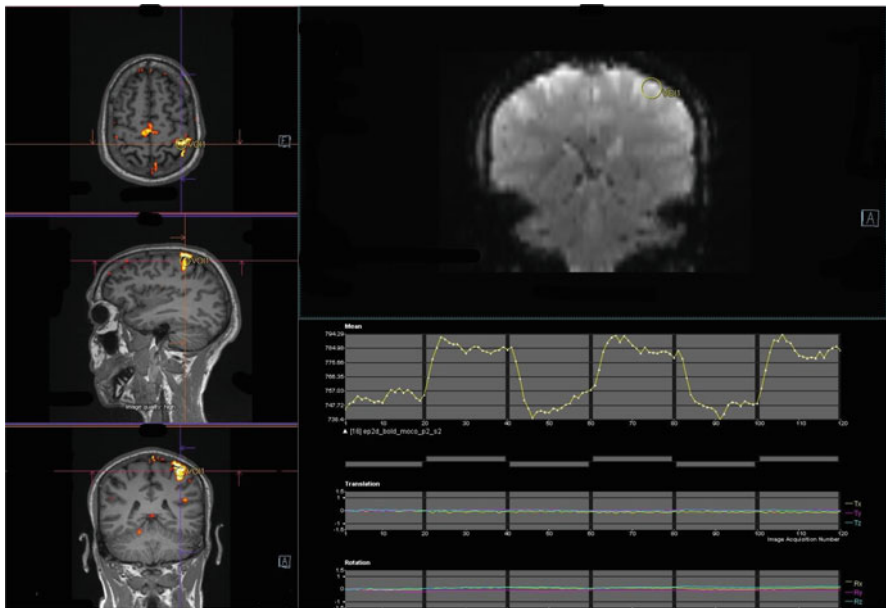

Fig. 9.8 Functional MRI showing activation of corresponding motor cortex with movement of right index finger

local dephasing of protons and thus reducing the signal returned from surrounding tissues. Heavy T_2^* weighted sequences are used for imaging in fMRI.

This imaging technique is used to look for the extent of involvement of eloquent areas (such as those involved in speech or motor function) by the tumour for presurgical planning.

9.4   Conclusion

Today MRI is not just limited to providing the anatomical details. Advanced MRI sequences also enable us to evaluate the metabolic and functional status of tissues at molecular level in a non-invasive manner. Use of advanced MRI techniques forms an essential component of diagnostic algorithm of neurological diseases both for diagnosis and assessment of response to treatment before anatomical changes set in.

Declaration All the figures described in the text have been obtained by the authors at their institute.

References

1. Bakshi R, Ariyaratana S, Benedict RHB, Jacobs L (2001) Fluid-attenuated inversion recovery magnetic resonance imaging detects cortical and juxtacortical multiple sclerosis lesions. Arch Neurol 58:742–748
2. Okuda T, Korogi Y, Ikushima I, Murakami R, Nakashima K, Yasunaga T, Kondo Y, Takahashi M (2014) Use of fluid-attenuated inversion recovery (FLAIR) pulse sequences in perinatal hypoxic-ischaemic encephalopathy. Br J Radiol 71:282–290. https://doi.org/10.1259/bjr718439616237
3. Bangerter NK, Hargreaves BA, Gold GE, Stucker DT, Nishimura DG (2006) Fluid-attenuated inversion-recovery SSFP imaging. J Magn Reson Imaging 24:1426–1431
4. Vaswani AK, Nizamani WM, Ali M, Aneel G, Shahani BK, Hussain S (2014) Diagnostic accuracy of contrast-enhanced FLAIR magnetic resonance imaging in diagnosis of meningitis correlated with CSF analysis. ISRN Radiol 2014:1–7
5. Moritani T, Ekholm S, Westesson PL (2009) Diffusion-weighted MR imaging of the brain, 2nd edn. Springer, New York, pp 1–401
6. Neurology | Handbook of Neurosurgery. https://www.thieme.com/books-main/neurology/product/5411-handbook-of-neurosurgery. Accessed 27 Sept 2021
7. Diffusion MRI: theory, methods, and applications—Oxford medicine. https://oxfordmedicine.com/view/10.1093/med/9780195369779.001.0001/med-9780195369779. Accessed 27 Sept 2021
8. Cha S (2006) Update on brain tumor imaging: from anatomy to physiology. Am J Neuroradiol 27:475–487. http://www.ajnr.org/content/27/3/475. Accessed 27 Sept 2021
9. Tong KA, Ashwal S, Obenaus A, Nickerson JP, Kido D, Haacke EM (2008) Susceptibility-weighted MR imaging: a review of clinical applications in children. Am J Neuroradiol 29:9–17
10. Haacke EM, Mittal S, Wu Z, Neelavalli J, Cheng Y-CN (2009) Susceptibility-weighted imaging: technical aspects and clinical applications, part 1. Am J Neuroradiol 30:19–30
11. Tong KA, Ashwal S, Holshouser BA, Nickerson JP, Wall CJ, Shutter LA, Osterdock RJ, Haacke EM, Kido D (2004) Diffuse axonal injury in children: clinical correlation with hemorrhagic lesions. Ann Neurol 56:36–50

12. Santhosh K, Kesavadas C, Thomas B, Gupta AK, Thamburaj K, Kapilamoorthy TR (2009) Susceptibility weighted imaging: a new tool in magnetic resonance imaging of stroke. Clin Radiol 64:74–83

13. Rosen BR, Belliveau JW, Chien D (1989) Perfusion imaging by nuclear magnetic resonance. Magn Reson Q 5:263–281

14. Essig M, Shiroishi MS, Nguyen TB et al (2013) Perfusion MRI: the five Most frequently asked technical questions. Am J Roentgenol 200:24–34. https://doi.org/10.2214/AJR129543

15. Petrella JR, Provenzale JM (2000) MR perfusion imaging of the brain: techniques and applications. AJR Am J Roentgenol 175:207–219

16. Petcharunpaisan S, Ramalho J, Castillo M (2010) Arterial spin labeling in neuroimaging. World J Radiol 2:384–398. http://www.wjgnet.com/

17. Sorensen AG, Buonanno FS, Gonzalez RG et al (1996) Hyperacute stroke: evaluation with combined multisection diffusion-weighted and hemodynamically weighted echo-planar MR imaging. Radiology 199:391–401. https://doi.org/10.1148/radiology19928668784

18. Sorensen AG, Copen WA, Østergaard L, Buonanno FS, Gonzalez RG, Rordorf G, Rosen BR, Schwamm LH, Weisskoff RM, Koroshetz WJ (1999) Hyperacute stroke: simultaneous measurement of relative cerebral blood volume, relative cerebral blood flow, and mean tissue transit time. Radiology 210:519–527. https://doi.org/10.1148/radiology2102.r99fe06519

19. Mattay VS, Frank JA, Duyn JH et al (1996) Three-dimensional "BURST" functional magnetic resonance imaging: initial clinical applications. Acad Radiol 3:S379–S383

20. Harris GJ, Lewis RF, Satlin A, English CD, Scott TM, Yurgelun-Todd DA, Renshaw PF (1998) Dynamic susceptibility contrast MR imaging of regional cerebral blood volume in Alzheimer disease: a promising alternative to nuclear medicine. Am J Neuroradiol 19(9):1727–1732

21. Simmons MLL, Frondoza CGG, Coyle JTT (1991) Immunocytochemical localization of N-acetyl-aspartate with monoclonal antibodies. Neuroscience 45:37–45

22. Reddy N, Calloni SF, Vernon HJ, Boltshauser E, Huisman TAGM, Soares BP (2018) Neuro-imaging findings of organic acidemias and aminoacidopathies. Radiographics 38:912–931. https://doi.org/10.1148/rg2018170042

23. Davie CA, Barker GJ, Tofts PS, Hawkins CP, Brennan A, Miller DH, Mcdonald WI (1993) Detection of myelin breakdown products by proton magnetic resonance spectroscopy. Lancet 341:630–631

24. Kreis R, Ross BD, Farrow NA, Ackerman Z (1992) Metabolic disorders of the brain in chronic hepatic encephalopathy detected with H-1 MR spectroscopy. Radiology 182:19–27. https://doi.org/10.1148/radiology18211345760

25. Penrice J, Cady EB, Lorek A, Wylezinska M, Amess PN, Aldridge RF, Stewart A, Wyatt JS, Reynolds EOR (1996) Proton magnetic resonance spectroscopy of the brain in normal preterm and term infants, and early changes after perinatal hypoxia-ischemia. Pediatr Res 401(40):6–14

26. Barker PB, Gillard JH, van Zijl PC, Soher BJ, Hanley DF, Agildere AM, Oppenheimer SM, Bryan RN (1994) Acute stroke: evaluation with serial proton MR spectroscopic imaging. Radiology 192:723–732. https://doi.org/10.1148/radiology19238058940

27. Petroff OAC, Graham GD, Blamire AM, Al-Rayess M, Rothman DL, Fayad PB, Brass LM, Shulman RG, Prichard JW (1992) Spectroscopic imaging of stroke in humans. Neurology 42:1349–1349

28. Alger JR, Frank JA, Bizzi A, Fulham MJ, DeSouza BX, Duhaney MO, Inscoe SW, Black JL, van Zijl PC, Moonen CT (1990) Metabolism of human gliomas: assessment with H-1 MR spectroscopy and F-18 fluorodeoxyglucose PET. Radiology 177:633–641. https://doi.org/10.1148/radiology17732243962

29. Lin DDM, Crawford TO, Barker PB, Morgan RH, Lin DM, Hopkins J (2003) Proton MR spectroscopy in the diagnostic evaluation of suspected mitochondrial disease. AJNR Am J Neuroradiol 24:33–41

30. Matthews PM, Andermann F, Silver K, Karpati G, Arnold DL (1993) Proton MR spectroscopic characterization of differences in regional brain metabolic abnormalities in mitochondrial encephalomyopathies. Neurology 43:2484–2484

31. Ross B, Michaelis T (1994) Clinical applications of magnetic resonance spectroscopy. Magn Reson Q 10:191–247
32. Shonk TK, Moats RA, Gifford P, Michaelis T, Mandigo JC, Izumi J, Ross BD (1995) Probable Alzheimer disease: diagnosis with proton MR spectroscopy. Radiology 195:65–72. https://doi.org/10.1148/radiology19517892497
33. Kruse B, Hanefeld F, Christen HJ, Bruhn H, Michaelis T, Hänicke W, Frahm J (1993) Alterations of brain metabolites in metachromatic leukodystrophy as detected by localized proton magnetic resonance spectroscopy in vivo. J Neurol 241:68–74
34. Magistretti PJ, Pellerin L, Rothman DL, Shulman RG (1999) Energy on demand. Science 283:496–497
35. Srinivasan R, Sailasuta N, Hurd R, Nelson S, Pelletier D (2005) Evidence of elevated glutamate in multiple sclerosis using magnetic resonance spectroscopy at 3 T. Brain 128:1016–1025
36. Kreis R, Pfenninger J, Herschkowitz N, Boesch C (1995) In vivo proton magnetic resonance spectroscopy in a case of Reye's syndrome. Intensive Care Med 21:266–269
37. Basser PJ, Mattiello J, LeBihan D (1994) Estimation of the effective self-diffusion tensor from the NMR spin echo. J Magn Reson B 103:247–254
38. Basser PJ, Mattiello J, LeBihan D (1994) MR diffusion tensor spectroscopy and imaging. Biophys J 66:259–267
39. Alexander AL, Eun Lee J, Lazar M, Field AS (2007) Diffusion tensor imaging of the brain. Neurotherapeutics 4:316–329
40. Mori S, Kaufmann WE, Davatzikos C et al (2002) Imaging cortical association tracts in the human brain using diffusion-tensor-based axonal tracking. Magn Reson Med 47:215–223
41. Catani M, Howard RJ, Pajevic S, Jones DK (2002) Virtual in vivo interactive dissection of white matter fasciculi in the human brain. NeuroImage 17:77–94
42. Stieltjes B, Kaufmann WE, van Zijl PCM, Fredericksen K, Pearlson GD, Solaiyappan M, Mori S (2001) Diffusion tensor imaging and axonal tracking in the human brainstem. NeuroImage 14:723–735
43. Wakana S, Jiang H, Nagae-Poetscher LM, van Zijl PCM, Mori S (2004) Fiber tract-based atlas of human white matter anatomy. Radiology 230:77–87. https://doi.org/10.1148/radiol2301021640
44. Jellison BJ, Field AS, Medow J, Lazar M, Salamat MS, Alexander AL (2004) Diffusion tensor imaging of cerebral white matter: a pictorial review of physics, fiber tract anatomy, and tumor imaging patterns. Am J Neuroradiol 25:356–369
45. Witwer BP, Moftakhar R, Hasan KM et al (2002) Diffusion-tensor imaging of white matter tracts in patients with cerebral neoplasm. J Neurosurg 97:568–575
46. Lazar M, Alexander AL, Thottakara PJ, Badie B, Field AS (2006) White matter reorganization after surgical resection of brain tumors and vascular malformations. Am J Neuroradiol 27:1258–1271
47. Laundre BJ, Jellison BJ, Badie B, Alexander AL, Field AS (2005) Diffusion tensor imaging of the corticospinal tract before and after mass resection as correlated with clinical motor findings: preliminary data. Am J Neuroradiol 26:791–796
48. Van Gelderen P, de Vleeschouwer MH, DesPres D, Pekar J, van Zijl PC, Moonen CT (1994) Water diffusion and acute stroke. Magn Reson Med 31:154–163
49. Liu Y, D'Arceuil HE, Westmoreland S, He J, Duggan M, Gonzalez RG, Pryor J, de Crespigny AJ (2007) Serial diffusion tensor MRI after transient and permanent cerebral ischemia in nonhuman primates. Stroke 38:138–145
50. Sorensen AG, Wu O, Copen WA, Davis TL, Gonzalez RG, Koroshetz WJ, Reese TG, Rosen BR, Wedeen VJ, Weisskoff RM (1999) Human acute cerebral ischemia: detection of changes in water diffusion anisotropy by using MR imaging. Radiology 212:785–792. https://doi.org/10.1148/radiology2123.r99se24785
51. Yang Q, Tress BM, Barber PA, Desmond PM, Darby DG, Gerraty RP, Li T, Davis SM (1999) Serial study of apparent diffusion coefficient and anisotropy in patients with acute stroke. Stroke 30:2382–2390

52. Beaulieu C, Allen PS (1994) Determinants of anisotropic water diffusion in nerves. Magn Reson Med 31:394–400
53. Henry RG, Oh J, Nelson SJ, Pelletier D (2003) Directional diffusion in relapsing-remitting multiple sclerosis: a possible in vivo signature of Wallerian degeneration. J Magn Reson Imaging 18:420–426
54. Choi SJ, Lim KO, Monteiro I, Reisberg B (2016) Diffusion tensor imaging of frontal white matter microstructure in early Alzheimer's disease: a preliminary study. J Geriat Psychiatry Neurol 18:12–19. https://doi.org/10.1177/0891988704271763
55. Assaf Y, Ben-Sira L, Constantini S, Chang LC, Beni-Adani L (2006) Diffusion tensor imaging in hydrocephalus: initial experience. AJNR Am J Neuroradiol 27:1717
56. Gross DW, Concha L, Beaulieu C (2006) Extratemporal white matter abnormalities in mesial temporal lobe epilepsy demonstrated with diffusion tensor imaging. Epilepsia 47:1360–1363
57. Moeller FG, Hasan KM, Steinberg JL, Kramer LA, Valdes I, Lai LY, Swann AC, Narayana PA (2007) Diffusion tensor imaging eigenvalues: preliminary evidence for altered myelin in cocaine dependence. Psychiatry Res Neuroimaging 154:253–258
58. Alexander AL, Lee JE et al (2006) Diffusion tensor imaging of the corpus callosum in autism. NeuroImage 34:61–73. https://doi.org/10.1016/j.neuroimage.2006.08.032
59. Moonen CTW, Chrit TW, Bandettini PA, Peter A, Aguirre GK, Geoffrey K (1999) Functional MRI. Springer, Berlin, p 575
60. Stippich C (2015) Clinical functional MRI: presurgical functional neuroimaging. Springer, Berlin, p 351